Reference: *Biol. Bull.* **185:** 393–404. (December, 1993)

A Comparative Study of Static Bodies in Mysid Crustaceans: Evolutionary Implications of Crystallographic Characteristics

A. P. ARIANI[1], K. J. WITTMANN[2], AND E. FRANCO[3]

[1]Dipartimento di Zoologia, Università di Napoli, Via Mezzocannone 8, I-80134 Napoli, Italia;
[2]Institut für Allgemeine Biologie, Universität Wien, Schwarzspanierstrasse 17, A-1090 Vienna,
Austria; and [3]Dipartimento di Scienze della Terra, Università di Napoli,
Via Mezzocannone 8, I-80134 Napoli, Italia

Abstract. We studied the mineral composition of statoliths in 154 species belonging to 55 genera of Mysidae. Fluorite (CaF_2) was found in 86% of Recent species, vaterite ($CaCO_3$) in 9%, and no crystalline component in 5%. Seven samples of fossil statoliths from Upper Miocene deposits were exclusively calcite ($CaCO_3$).

Vaterite has the peak of occurrence in fresh water, fluorite in the photic zone of marine waters, and organic statoliths in oceanic deep waters. With respect to population numbers in the different aquatic biota, vaterite prevails in freshwater species and fluorite is dominant among species in all brackish to marine environments.

The occurrence of $CaCO_3$ in fresh to brackish waters coincides with fossil records and biogeographical observations. The Ponto-Caspian region is the center of abundance for Recent $CaCO_3$-precipitating species. The rich brackish to freshwater fauna in this region probably has its roots in the brackish Paratethys, where a rich fossil material of calcareous mysid statoliths is known from Upper Miocene sediments.

Morphological and scarce palaeontological evidence suggests that the earliest (Carboniferous to Jurassic) Mysidacea were mainly oceanic shrimps without statocysts; these were followed by (bentho)pelagic animals with nonmineralic organic statoliths. With the colonization of coastal to littoral areas by benthopelagic to benthic forms, mineralic statoliths were formed by precipitation of fluorite. Among the modern Mysidae, a special development occurred (in the Miocene) in the Ponto-Caspian region where $CaCO_3$ statoliths appeared in brackish to freshwater forms.

As in vertebrates, the patterns of mineral composition of static bodies in the Mysidae reflect both anatomical and ecophysiological differences.

Introduction

The hard parts of animals consist of a variety of minerals, some of which occur in static organs (statocysts) as components of the static bodies, statoliths, or otoliths (Lowenstam, 1981). Carlström (1963) first showed that in vertebrates, the mineral composition of otoliths provides evolutionary information: the primitive forms (Agnatha) have phosphatic otoliths, but in the Gnathostomata, all endogenous otoliths consist of calcium carbonate. The form of the latter varies from vaterite in primitive bony fishes (Chondrostei Acipenseroidea) to more stable polymorphs—aragonite in advanced bony fishes and amphibians, both aragonite and calcite in reptiles, and only calcite in birds and mammals. Later investigations (Marmo *et al.*, 1983; Gauldie, 1990) modified only the details of this picture.

By analogy to the investigations on vertebrates, we sought to identify possible evolutionary implications of the mineral composition of statoliths in a group of invertebrates. Unlike most crustaceans, which have exogenous static bodies, mysid shrimps of the family Mysidae have large endogenous statoliths in a pair of statocyst chambers on the base of the tail fan. The statocysts serve as the primary equilibrium organs for these small shrimps, which spend a substantial portion of their lives swimming. Each statocyst chamber contains a single statolith, a

Received 15 April 1993; accepted 31 August 1993.

moveable dense body, which transmits gravitational and inertial forces as primary stimuli to attached sensory hairs. Besides controlling body position, the statocysts are also involved in stabilizing the visual perceptive field (Neil, 1975). In addition to gravity, light is important for the control of body position and swimming plane in mysids (Jander, 1962).

Mysid statoliths are of interest because in most species they consist of fluorite (CaF_2), a mineral that rarely occurs in the hard parts of organisms (Bethe, 1895; Lowenstam and McConnell, 1968). It may be of equal interest that certain species possess statoliths made of vaterite (Ariani *et al.*, 1981, 1983), a metastable polymorph of $CaCO_3$ that is rare in organisms and almost unknown from geologic systems. Fossil statoliths, however, consist of calcite (Voicu, 1974, 1981), the most common and stable phase of crystalline calcium carbonate.

During the last decade the following picture was obtained on the basis of a relatively modest number of extant species: statoliths composed of fluorite in the majority of marine species; vaterite in some representatives of the tribe Mysini, mainly in brackish to freshwater forms; and nonmineralic material in a few mesopelagic forms (Ariani *et al.*, 1983; Wittmann *et al.*, 1993). These results prompted the present large-scale study of the ecological, biogeographic, and evolutionary implications of crystallographic characteristics in a rich collection of material covering a broad range of taxonomic relationships, environments, and geographical areas.

Materials and Methods

The mysids were collected during the last two decades by means of plankton or bottom nets in fresh to marine waters around the globe. Materials were either fixed in 70% alcohol or briefly placed in a solution of 4–5% formaldehyde in ambient water, then transferred to 70% alcohol. Materials were examined a few hours to several years after collection. In some cases, especially for euryhaline species, specimens from different natural populations were examined. We studied 179 populations belonging to 154 species and 55 genera of extant mysids and also examined seven samples of fossil statoliths from Upper Miocene deposits of various parts of the Paratethys. Mysid statoliths from these sediments were assigned to the Recent genus *Paramysis* by Voicu (1981) and later transferred to the Miocene genus *Sarmysis* by Maissuradze and Popescu (1987).

Statoliths of extant species were mechanically removed from the endopods of uropods and briefly washed in distilled water. Statolith diameter was calculated as the geometric mean of apparent length and width in ventral view. Body length was measured with a micrometer eyepiece from the tip of the rostrum to the telson. We measured both body length and diameter from adults of both sexes: 5–20 individuals for most species, or only 1–4 specimens for very rare species. From the sediment samples we measured 5–10 fossil statoliths at each location.

In 96 extant species and 7 fossil samples, the mineral composition of crystalline components was determined by x-ray diffraction analysis on whole statoliths. The standard grinding of the samples to powder was not necessary because all crystalline statoliths gave clear diffraction patterns due to spherulitic microcrystal arrangement visible by transmitted light. Statoliths were glued with collodion to the tip of glass fibers. In the case of very small statoliths, up to four of them were put together on the same fiber. Diffraction patterns were recorded with a 114.6-mm Debye-Scherrer camera using Ni-filtered Cu-Kα radiation; working conditions: 40 kV, 30 mA, recording time 8–12 h. Diffractions that gave no lines were repeated with 24-h exposure.

In 102 species, a less expensive and faster method of mineral determination was used, as proposed by Wittmann *et al.* (1993). This method, which we call WSA, uses CH_3COOH treatment and inspection of crystal aggregates with polarization, scanning microscopy, or both, to identify statoliths by means of their chemical and physical characteristics. The four known types of statolith composition are distinguished without error, but new types may not always be detected or may not be well identified. From two to five statoliths of each species were examined. In 44 species both methods (X + WSA) were used and gave identical results.

Micrographs were obtained with a Cambridge Stereoscan scanning electron microscope (SEM) or with a JEOL SEM 35CF on parts or entire statoliths coated with gold. For qualitative SEM microanalysis, statoliths were briefly washed in distilled water twice and then air dried and carbon coated. Statoliths of 2–6 individuals in 10 species were analyzed with a LINK AN 10000 system. Elements with an order number ≥ 9 were recorded.

Results

The types of statoliths we identified were noncrystalline (organic) (Fig. 1), fluorite (Figs. 2, 3), vaterite (Figs. 4–6), and calcite (Figs. 7, 8). Eighty-six percent of Recent statoliths were mineralized with fluorite and only 9% with vaterite; 5% had no crystalline component (Table I). All fossil statoliths consisted of calcite (Table II).

Some statoliths gave no diffraction patterns—these showed elastic consistency and shrinkage due to desiccation. When observed in the animal, they resembled the spherical organic matrix that appears during the first stage of statolith formation (Ariani *et al.*, 1982). Fluorite showed its typical cubic habit (Fig. 3) at the statolith surface. Vaterite usually appeared as a patchwork of scales, needles,

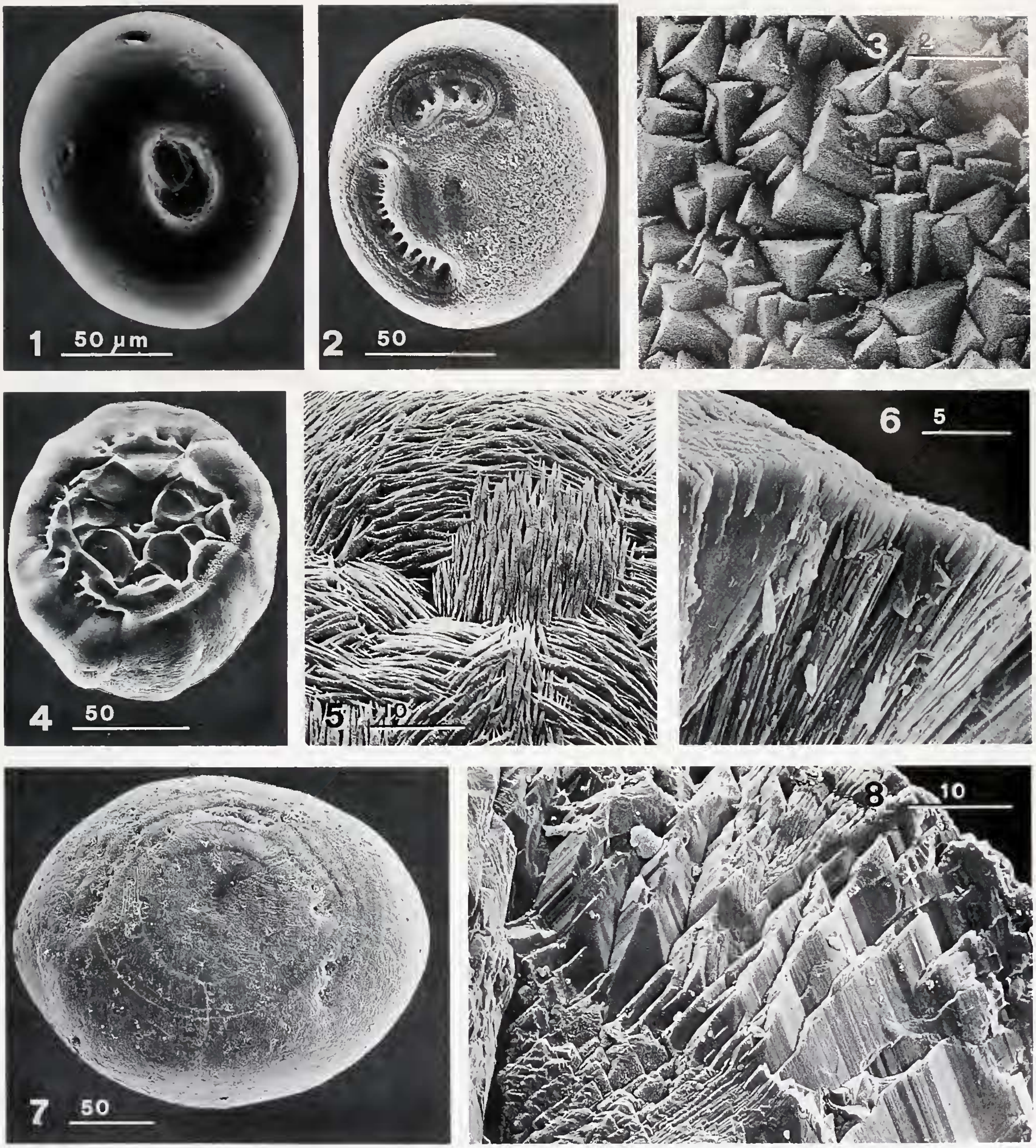

Figures 1–8. Mineral types of statoliths of Recent and fossil Mysidae: scanning electron micrographs of entire statoliths in ventral to ventrolateral view.

Figure 1. Noncrystalline statolith of *Boreomysis megalops*, center malformed due to desiccation.

Figure 2. Fluorite statolith of *Paramysis arenosa*.

Figure 3. *P. arenosa*, cubic habit of fluorite on ventral surface.

Figure 4. Vaterite statolith of *Paramysis helleri*.

Figure 5. *P. helleri*, aggregates of vaterite on dorsal surface.

Figure 6. *P. helleri*, lamellar habit of vaterite on fracture surface.

Figure 7. Fossil statolith from Upper Miocene sediments in the Oas Basin.

Figure 8. Fossil statolith, crystal habit of calcite on fracture surface.

Table I

Crystalline components of statoliths in Recent Mysidae

Species	Locality, remarks	Salinity ‰	Depth (m)	Body length[1] (mm)	Statol. diam.[1] (μm)	Method[2]	Crystall. component
Subfam. Boreomysinae							
Boreomysis arctica (Krøyer)	Korsfjorden, Norway	35	200	21	170	X + WSA	None
Boreomysis brucei W. Tattersall	Weddell Sea, Antarctic	35	980–990	35	110	WSA	None
Boreomysis megalops Sars	Tyrrhenian Sea, off Sardinia	36	330–400	11	160	X + WSA	None
	Hjeltefjord, Norway	35	260	13	150	X-ray	None
Boreomysis microps Sars	Biscay Depth, NE-Atlantic	35	500–1000	14	120	X + WSA	None
Boreomysis sphaerops Ii	N-Pacific, off Japan	35	≤850	22	200	WSA	None
Boreomysis tridens Sars	Norway, continental shelf	35	520	26	130	X-ray	None
Subfam. Siriellinae							
Siriella aequiremis Hansen	N-Pacific, off Christmas Island	35	Surface	8	310	X-ray	Fluorite
Siriella anomala Hansen	Batbatan, Philippines	35	10	10	290	X-ray	Fluorite
Siriella armata (M.-Edw.)	Gulf of Trieste, Adriatic	32–36	0–1	15	240	X + WSA	Fluorite
Siriella brevicaudata Paulson	Gulf of Aqaba, Red Sea	42	1–2	5	90	WSA	Fluorite
Siriella castellabatensis Ariani & Spagnuolo	Gulf of Salerno, Tyrrhenian Sea	38	<30	7	130	X-ray	Fluorite
Siriella clausii Sars	Gulf of Salerno, Tyrrhenian Sea	38	<30	6	150	X-ray	Fluorite
	Lake Faro, Sicily	33	<5	5	120	X-ray	Fluorite
Siriella gracilis Dana	Gulf of Aden, NE-Indian Ocean	36	Surface	5	130	WSA	Fluorite
	N-Pacific, off Philippines	34–35	Surface	5	130	WSA	Fluorite
Siriella inornata Hansen	Philippines, Batbatan	33–34	Coastal	11	190	WSA	Fluorite
Siriella jaltensis gracilipes Nouvel	Gulf of Salerno, Tyrrhenian Sea	38	<60	9	190	X + WSA	Fluorite
Siriella longipes Nakazawa	Kominato, Japan	33–35	20	14	250	X + WSA	Fluorite
Siriella norvegica Sars	Istria, N-Adriatic Sea	36	1	8	160	WSA	Fluorite
Siriella pacifica Holmes	Aqua Verde Bay, Gulf of California	35	10	10	230	X-ray	Fluorite
Siriella roosevelti W. Tattersall	Charles I., Galapagos Islands	35	10	7	170	WSA	Fluorite
Siriella thompsoni M.-Edw.	Gulf of Aden, NE-Indian Ocean	36	Surface	9	260	WSA	Fluorite
	Argentinian Basin, S-Atlantic	35	Surface	10	190	WSA	Fluorite
	N-Pacific, off Philippines	34–35	Surface	7	190	X-ray	Fluorite
Siriella trispina Ii	East China Sea	33–35	Surface	10	190	WSA	Fluorite
Siriella vulgaris rostrata W. Tattersall	Philippines, Batbatan	33–34	Surface	7	170	WSA	Fluorite
Subfam. Rhopalophthalminae							
Rhopalophthalmus terranatalis O. Tattersall	Algoa Bay, South Africa	10–34	0–6	14	200	X + WSA	None
Subfam. Gastrosaccinae							
Anchialina agilis (Sars)	Gulf of Salerno, Tyrrhenian Sea	38	20	6	70	X-ray	Fluorite
Anchialina oculata Hoenigman	Gulf of Salerno, Tyrrhenian Sea	38	<60	5	60	WSA	Fluorite
Gastrosaccus mediterraneus Bacescu	Adriatic, near Brindisi, littoral	38	0	7	80	X + WSA	Fluorite
Gastrosaccus roscoffensis Bacescu	English Channel, near Roscoff	35	<20	8	80	X-ray	Fluorite
Gastrosaccus sanctus sanctus (van Beneden)	Gulf of Salerno, Tyrrhenian Sea	32–38	2–16	8	70	X + WSA	Fluorite
Gastrosaccus sanctus widhalmi Bacescu	Black Sea, Romania	17	2	10	90	WSA	Fluorite
Gastrosaccus spinifer (Goës)	German Bight, North Sea	34–35	50–60	14	90	WSA	Fluorite
Haplostylus bacescui Hatzakis	Gulf of Salerno, Tyrrhenian Sea	38	12–19	8	130	X + WSA	Fluorite

Table 1 (*Continued*)

Species	Locality, remarks	Salinity ‰	Depth (m)	Body length[1] (mm)	Statol. diam.[1] (μm)	Method[2]	Crystall. component
Subfam. Gastrosaccinae (*Continued*)							
Haplostylus lobatus (Nouvel)	Gulf of Salerno, Tyrrhenian Sea	38	30–40	8	120	X + WSA	Fluorite
Haplostylus magnilobatus (Bacescu & Schieckc)	Gulf of Naples, Tyrrhenian Sea	36	35–40	8	100	X-ray	Fluorite
Haplostylus normani (Sars)	Gulf of Salerno, Tyrrhenian Sea	38	12–20	7	130	WSA	Fluorite
Subfam. Mysinae, tribe Erythropini							
Amblyops abbreviata (Sars)	Hjeltefjord, Norway	35	260	11	230	X + WSA	Fluorite
Amblyops antarctica O. Tattersall	Weddell Sea, Antarctic	35	470	14	200	WSA	Fluorite
Amblyops tattersalli Zimmer	Weddell Sea, Antarctic	35	520	25	360	WSA	Fluorite
Caesaromysis hispida Ortmann	N-Pacific, off Japan	34	≤1060	9	110	X-ray	Fluorite
Dactylamblyops hodgsoni Holt & Tattersall	Weddell Sea, Antarctica	35	400–600	21	300	X + WSA	Fluorite
Dactylamblyops iii Nouvel & Lagardere	N-Pacific, off Japan	34	≤1300	9	230	X-ray	Fluorite
Dactylamblyops murrayi W. Tattersall	N-Pacific, off Japan	34	≤480	12	230	X-ray	Fluorite
Erythrops elegans (Sars)	Gulf of Salerno, Tyrrhenian Sea	38	16	3	120	X + WSA	Fluorite
Erythrops microps (Sars)	Rockall Trough Area, N-Atlantic	35	700	7	170	X-ray	Fluorite
Erythrops neapolitana Colosi	Adriatic, Dalmatia	38	200	5	130	X-ray	Fluorite
Erythrops serrata (Sars)	Hjeltefjord, Norway	35	260	9	180	X-ray	Fluorite
Euchaetomera glyphidophthalmica Illig	N-Pacific, off Japan	35	≤1050	5	210	X-ray	Fluorite
Euchaetomera tenuis Sars	N-Pacific, off Japan	35	≤1250	9	240	WSA	Fluorite
Euchaetomera typica Sars	N-Pacific, off Japan	35	≤950	7	180	X-ray	Fluorite
Euchaetomera zurstrasseni (Illig)	Weddell Sea, Antarctica	35	140–300	8	210	WSA	Fluorite
Holmesiella affinis Ii	Honshu, Japan	34–35	72	11	300	X-ray	Fluorite
Illigiella brevisquamosa (Illig)	Honshu, Japan	33–34	280	8	160	X-ray	Fluorite
Katerythrops oceanae Holt & Tattersall	N-Pacific, off Japan	34–35	≤680	8	90	X-ray	Fluorite
Meterythrops microphthalma W. Tattersall	Sea of Japan	34	570–730	18	340	X + WSA	Fluorite
Meterythrops picta Holt & Tattersall	Rockall Trough Area, N-Atlantic	35	1500–2000	12	150	X-ray	Fluorite
	N-Pacific, off Japan	34	≤1300	13	140	X-ray	Fluorite
Paramblyops brevirostris O. Tattersall	Weddell Sea, Antarctic	35	350–380	15	280	WSA	Fluorite
Pseudamplyops conicops Ii	N-Pacific, off Japan	34	≤1300	11	110	X-ray	Fluorite
Pseudomma affine Sars	Hjeltefjord, Norway	35	260	8	130	X + WSA	Fluorite
Pseudomma armatum Hansen	Weddell Sea, Antarctic	35	250	21	290	WSA	Fluorite
Pseudomma belgicae (Hansen) [in Holt & Tatt.]	Weddell Sea, Antarctic	35	240	9	220	WSA	Fluorite
Pseudomma japonicum Murano	Honshu, Japan	33–35	72	4	90	X-ray	Fluorite
Pseudomma latiphthalmum Murano	Honshu, Japan	33–35	280	6	90	X-ray	Fluorite
Pseudomma roseum Sars	Fensfjord, Norway	35	460	14	190	X-ray	Fluorite
Teraterythrops robusta (Birstein & Tchindonova)	N-Pacific, off Japan	34	≤1440	5	100	WSA	Fluorite
Subfam. Mysinae, tribe Leptomysini							
Antichthomysis notidana Fenton	Beach near Hobart, SE-Tasmania	35	Coastal	9	240	WSA	Fluorite

Table I (*Continued*)

Species	Locality, remarks	Salinity ‰	Depth (m)	Body length[1] (mm)	Statol. diam.[1] (μm)	Method[2]	Crystall. component
Subfam. Mysinae, tribe Leptomysini (*Continued*)							
Leptomysis buergii Bacescu	Gulf of Taranto, Ionian Sea	38	5	8	230	X + WSA	Fluorite
Leptomysis gracilis (Sars)	Gulf of Biscay, NE-Atlantic	35	90	9	190	WSA	Fluorite
Leptomysis heterophila Wittmann	Istria, N-Adriatic Sea	34–37	17	8	190	WSA	Fluorite
Leptomysis lingvura adriatica Wittmann	Gulf of Taranto, Ionian Sea	38	2	6	180	X + WSA	Fluorite
Leptomysis lingvura marioni (Gourret)	Gulf of Naples, Tyrrhenian Sea	35–37	8–12	7	190	WSA	Fluorite
Leptomysis mediterranea atlantica Wittmann	Gulf of Biscay, NE-Atlantic	35	<10	11	240	WSA	Fluorite
Leptomysis mediterranea mediterranea Sars	Gulf of Salerno, Tyrrhenian Sea	28–36	2–4	9	270	WSA	Fluorite
Leptomysis megalops Zimmer	Gulf of Biscay, NE-Atlantic	35	180	9	220	X-ray	Fluorite
Leptomysis posidoniae Wittmann	Gulf of Naples, Tyrrhenian Sea	35–37	12	7	180	X + WSA	Fluorite
Leptomysis truncata sardica (Sars)	Gulf of Naples, Tyrrhenian Sea	35–37	1–2	9	230	WSA	Fluorite
Leptomysis truncata truncata (Heller)	Gulf of Triest, N-Adriatic Sea	32–36	0–1	8	230	WSA	Fluorite
Metamysidopsis swifti Bacescu	Tampa Bay, Florida	35	20	6	110	X-ray	Fluorite
Mysideis insignis (Sars)	Hjeltefjord, Norway	35	260	16	270	X-ray	Fluorite
Mysideis parva Zimmer	Adriatic, near Ancona	37	225	9	230	X-ray	Fluorite
Mysidetes posthon Holt & Tattersall	Weddell Sea, Antarctic	35	400–500	28	340	WSA	Fluorite
Mysidopsis acuta Hansen	S-Atlantic, off Falkland Islands	34	≤150	10	260	WSA	Fluorite
Mysidopsis almyra Bowman	Everglades, Florida	10	1	7	160	WSA	Fluorite
Mysidopsis bahia Molenok	Lab. tanks, from Gulf of Mexico	30	Coastal	7	110	X-ray	Fluorite
Mysidopsis bigelowi W. Tattersall	NW-Atlantic, off North Carolina	32	23	6	190	WSA	Fluorite
Mysidopsis gibbosa Sars	Gulf of Trieste, Adriatic	36	22	3	120	X + WSA	Fluorite
Notomysis australiensis (W. Tattersall)	St. Vincent Gulf, South Australia	35	9–11	10	310	X-ray	Fluorite
Paraleptomysis banyulensis (Bacescu)	Gulf of Salerno, Tyrrhenian Sea	38	16	7	230	X + WSA	Fluorite
Paraleptomysis dimorpha Wittmann	Cape Lopez area, Gabon, W-Africa	34	60–70	7	160	WSA	Fluorite
Prionomysis sp.	Storm Bay, Hope Beach, SE-Tasmania	35	Coastal	9	310	X-ray	Fluorite
Pseudomysis dactylops W. Tattersall	Honshu, Japan	33–35	275	13	200	X + WSA	Fluorite
Pyroleptomysis rubra Wittmann	Gulf of Eilat, Red Sea	42	Coastal	5	150	WSA	Fluorite
	Gulf of Trieste, Adriatic	34–37	6	7	200	X-ray	Fluorite
Tenagomysis tasmaniae Fenton	Derwent River, SE-Tasmania	35	Coastal	9	230	WSA	Fluorite
Subfam. Mysinae, tribe Mysini							
Acanthomysis dybowskii Ii	Bering Sea	33	37	22	450	WSA	Fluorite
Acanthomysis japonica (Marukawa)	Kominato, Japan	30–34	Coastal	11	290	WSA	Fluorite
Acanthomysis longicornis (M.-Edw.)	Gulf of Trieste, Adriatic	36	10–28	5	120	X + WSA	Fluorite
Acanthomysis macropsis (W. Tattersall)	San Francisco Bay	34	9	11	200	WSA	Fluorite
Acanthomysis mitsukurii Ii	Tateyama Bay, Japan	30–34	20	9	180	X-ray	Fluorite
Acanthomysis nakazatoi Ii	Tateyama Bay, Japan	30–34	20	14	240	X-ray	Fluorite

Table 1 (*Continued*)

Species	Locality, remarks	Salinity ‰	Depth (m)	Body length[1] (mm)	Statol. diam.[1] (μm)	Method[2]	Crystall. component
Subfam. Mysinae, tribe Mysini (*Continued*)							
Acanthomysis tamurai Ii	Tateyama Bay, Japan	30–34	Coastal	11	270	WSA	Fluorite
Anisomysis ijimai Nakazawa	Heta, Japan	30–34	Surface	7	120	WSA	Fluorite
Anisomysis marisrubri Bacescu	Gulf of Aqaba, Red Sea	42	0–3	5	100	WSA	Fluorite
Anisomysis sp.	N-Red Sea, near Sharm el Sheikh	42	1–2	3	60	WSA	Fluorite
Antarctomysis maxima (Hansen) [in Holt & Tatt.]	Weddell Sea, Antarctic	35	300–490	60	690	X + WSA	Fluorite
Antarctomysis ohlinii Hansen	Weddell Sea, Antarctic	35	≤850	64	560	X + WSA	Fluorite
Antromysis cenotensis Creaser	Cave of Tzab-Nah, Yucatan, Mexico	0	1	3	60	X-ray	Vaterite
Diamysis bahirensis (Sars)	Lake of Tunis	38	1	4	130	X-ray	Vaterite
	Gulf of Naples, Tyrrhenian Sea	37	20	5	120	X + WSA	Vaterite
	Piccolo river, Apulia, S-Italy	11–13	1	7	140	X + WSA	Vaterite
	San Pietro river, Apulia, S-Italy	3–5	1	7	140	X-ray	Vaterite
	Lake Deransko, Bosnia-Hercegovina	0	0–1	7	160	X-ray	Vaterite
Diamysis pengoi (Czerniavsky)	Danube Delta, Romania	0	3	9	180	X-ray	Fluorite
Hemimysis abyssicola Sars	Hjeltefjord, Norway	35	260	11	170	X-ray	Fluorite
Hemimysis anomala Sars	Northern Baltic Sea, Finland	<7	Lower litt.	7	160	WSA	Vaterite
Hemimysis lamornae lamornae (Couch)	Norway, Kristineberg	35	15	5	110	WSA	Fluorite
Hemimysis lamornae mediterranea Bacescu	Gulf of Naples, Tyrrhenian Sea	37	1–3	6	130	X + WSA	Fluorite
Hemimysis speluncola Ledoyer	N-Adriatic, near Rovinj	37	2	7	130	X-ray	Fluorite
Holmesimysis costata (Holmes)	Monterey Bay, California	35	20	10	170	X-ray	Fluorite
Idiomysis tsurnamali Bacescu	Gulf of Eilat, Red Sea	38	30	3	110	X-ray	Fluorite
Kainommatomysis schieckei Bacescu	N-Red Sea, near Sharm el Sheikh	42	1–2	3	120	WSA	Fluorite
Katamysis warpachowskyi Sars	Danube Delta, Romania	0	3	8	100	X-ray	Vaterite
Limnomysis benedeni Czerniavsky	Lake Sinoe, Danube Delta	2	0–1	10	160	WSA	Vaterite
	Danube in Vienna	0	0–1	9	150	X + WSA	Vaterite
Mesopodopsis aegyptia Wittmann	Island of Lesbos, Aegean Sea	39	3	6	170	WSA	Fluorite
Mesopodopsis orientalis (W. Tattersall)	Banica, Philippines	7	Surface	7	180	WSA	Fluorite
Mesopodopsis slabberi (van Beneden)	Lake of Tunis	38–40	1	9	160	X-ray	Fluorite
	Gulf of Taranto, Ionian Sea	35	1	9	120	WSA	Fluorite
	Penzé Estuary, English Channel	4–17	<1	11	190	WSA	Fluorite
	Costinesti, Black Sea	13	2	11	190	WSA	Fluorite
	Lake Sinoe, Danube Delta	2	0–1	10	170	X-ray	Fluorite
Mesopodopsis wooldridgei Wittmann	Algoa Bay, South Africa	10–34	3	10	170	X + WSA	Fluorite
Mysidium columbiae (Zimmer)	Stann Creek District, Belize	35	1	6	130	WSA	Fluorite
Mysidium integrum W. Tattersall	English Harbour, Antigua, W-Indies	35	2	6	130	X + WSA	Fluorite
Mysis litoralis (Banner)	Arctic Ocean, off P. Barrow, Alaska	35	20	12	170	WSA	Fluorite
Mysis mixta Lilljeborg	Massachusetts Bay	10	1	13	280	X-ray	Fluorite
Mysis relicta Lovén	Lake near Drottningholm, Sweden	0	20	12	180	X + WSA	Fluorite
	Green Lake, Wisconsin	0	55–120	18	220	X-ray	Fluorite

Table I (*Continued*)

Species	Locality, remarks	Salinity ‰	Depth (m)	Body length[1] (mm)	Statol. diam.[1] (μm)	Method[2]	Crystall. component
Subfam. Mysinae, tribe Mysini (*Continued*)							
Neomysis americana (Smith)	Oregon Inlet, North Carolina	32–34	Coastal	8	200	WSA	Fluorite
Neomysis integer (Leach)	Baltic Sea, Askö I., Sweden	7	0–1	11	220	X + WSA	Fluorite
Neomysis japonica Nakazawa	Tokyo Bay	<15	1	13	190	X-ray	Fluorite
Neomysis mercedis Holmes	San Francisco Bay	35	10–14	11	200	WSA	Fluorite
Neomysis rayii (Murdoch)	San Francisco Bay	34	9	28	380	WSA	Fluorite
Paramesopodopsis rufa Fenton	Derwent River, SE-Tasmania	35	Coastal	10	210	X-ray	Fluorite
Paramysis arenosa (Sars)	Gulf of Salerno, Tyrrhenian Sea	38	4–16	6	140	X + WSA	Fluorite
	Firth of Lorne, Scottish Sea	32–35	0–1	7	130	X-ray	Fluorite
Paramysis bacescoi Labat	Guernsey, Channel Islands	35	10	7	180	X-ray	Vaterite
Paramysis helleri (Sars)	S-Adriatic, near Brindisi	38	1	7	140	X + WSA	Vaterite
	Small creek near Split, Dalmatia	0	<1	9	150	WSA	Vaterite
Paramysis intermedia (Czerniavsky)	Danube Delta, Romania	0	0–1	11	140	X + WSA	Vaterite
Paramysis kessleri sarsi (Derjavin)	Danube Delta, Romania	0	0–1	5	140	X-ray	Vaterite
Paramysis kroeyeri (Czerniavsky)	Lake Uluabat, NW-Turkey	0	0–1	9	140	X-ray	Vaterite
Paramysis lacustris tanaitica (Martinov)	Danube Delta, Romania	0	3	14	160	X + WSA	Vaterite
Paramysis nouveli Labat	Small river, Roscoff, Eng. Channel	5–33	0	9	180	X-ray	Vaterite
Paramysis pontica Bacescu	Altintas Bay, Marmara Sea	19	35	8	180	X-ray	Vaterite
Praunus flexuosus (Müller)	Roscoff, English Channel	26–35	0	18	180	X + WSA	Fluorite
Praunus inermis (Rathke)	Firth of Lorne, Scottish Sea	32–35	1–5	11	180	WSA	Fluorite
Praunus neglectus (Sars)	Roscoff, English Channel	26–35	1	19	320	WSA	Fluorite
Proneomysis perminuta Ii	Tateyama Bay, Japan	33–35	Coastal	7	210	WSA	Fluorite
Proneomysis toriumii Murano	Tateyama Bay, Japan	33–35	Coastal	9	180	WSA	Fluorite
Schistomysis assimilis (Sars)	Gulf of Salerno, Tyrrhenian Sea	24–37	2–6	9	290	X + WSA	Vaterite
	Lagoon near Caorle, Gulf of Venice	11	0	9	230	WSA	Vaterite
Schistomysis kervillei (Sars)	North Sea, German coast	35	<50	13	240	WSA	Fluorite
Schistomysis ornata (Sars)	Gulf of Biscay, NE-Atlantic	35	<100	12	280	X-ray	Fluorite
Schistomysis spiritus (Norman)	English Channel, near Roscoff	35	10	12	210	X + WSA	Fluorite
Taphromysis bowmani Bacescu	Wakulla, Florida	10	1	8	120	WSA	Fluorite
Taphromysis louisianae Banner	Blackwater River, Florida	1	<2	9	120	WSA	Fluorite
Tasmanomysis oculata Fenton	Catamaran River, SE-Tasmania	35	Coastal	11	200	WSA	Fluorite
Troglomysis vjetrenicensis Stammer	Cave of Vjetrenica, Hercegovina	0	0–1	13	150	X-ray	Fluorite
Subfam. Mysinae, tribe Heteromysini							
Heteromysis formosa Smith	Narragansett Bay, Rhode Island	32	Coastal	6	130	X + WSA	Fluorite
Heteromysis mayana Brattegard	Coral reef aquarium, Smith. Inst.	35	Coastal	4	90	X-ray	Fluorite
Heteromysis microps (Sars)	Gulf of Naples, Tyrrhenian Sea	35–37	3	6	110	WSA	Fluorite
Heteromysis sp.	Weddell Sea, Antarctic	35	210–250	17	140	WSA	Fluorite
Subfam. Mysidellinae							
Mysidella typica Sars	Hjeltefjord, Norway	35	260	6	100	X + WSA	Fluorite
Mysidella sp.	Weddell Sea, Antarctic	35	280	7	70	WSA	Fluorite

[1] Values are the means of statoliths from either 5–20 or (for very rare species) 1–4 adult male and female specimens.

[2] X-ray = X-ray diffraction; WSA = the WSA method (Wittmann *et al.*, 1993); X + WSA = both methods.

Table II

Crystalline components of statoliths of Mysidae Mysini from Miocene (Upper Vollhynian to Lower Bessarabian) sediments of the brackish Paratethys

Location	Diameter[1] (μm)	Method[2]	Crystalline component
Carpathian Foredeep, Machów, Poland	190	X-ray	Calcite
Carpathian Foredeep, Berca, Romania	200	X-ray	Calcite
Carpathian Foredeep, Dacic Basin, Romania	220	X-ray	Calcite
Oas Basin, Transylvania, Romania	230	X-ray	Calcite
Transylvanian Basin, Ocna Mures, Romania	190	X + WSA	Calcite
Eastern Caucasian Foredeep, Tul'skaya, former USSR	180	X + WSA	Calcite
Kerch Peninsula, Kop-Takyl, former USSR	210	X + WSA	Calcite

[1] Values are the means of 5–10 statoliths.

[2] X-ray = X-ray diffraction; X + WSA = both X-ray diffraction and the WSA method (Wittmann *et al.*, 1993).

or lens-like aggregates (Fig. 5), but occasionally occurred as nodules. Fractures of both fluorite and vaterite statoliths showed scales in a spherulitic arrangement (Fig. 6). Fractures and, less frequently, surfaces of fossil statoliths showed characteristic calcite crystal forms (Fig. 8).

In noncrystalline (*Rhopalophthalmus terranatalis*), fluorite (*Leptomysis lingvura adriatica, Mesopodopsis slabberi, Neomysis integer*), and vaterite (*Diamysis bahirensis, Limnomysis benedeni*) statoliths, no difference in mineral composition was found between freshly caught individuals and conspecific material that had been stored for several years.

Noncrystalline statoliths appeared to be confined to the subfamilies Boreomysinae and Rhopalophthalminae. Fluorite statoliths were characteristic of Siriellinae, Gastrosaccinae, Mysidellinae, and most Mysinae. Vaterite statoliths were restricted to certain representatives of the tribe Mysini (Mysinae). In *Diamysis, Paramysis* (Figs. 2–6), *Schistomysis*, and *Hemimysis*, congeneric species showed either fluorite or vaterite.

In spite of the large interspecific variability, no intraspecific variations in mineral type were found (Table I). This was true for extremely euryhaline species (*Paramysis helleri, Diamysis bahirensis*, and *Mesopodopsis slabberi*) and for distant populations of *Siriella thompsoni* (South Atlantic, northeast Indian Ocean, and North Pacific), *Meterythrops picta* (North Atlantic and North Pacific), and *Mysis relicta* (northern Europe and North America). Similarly, no differences were found between the sexes or between left and right statoliths.

The ecological distribution of statolith mineral composition is summarized in Table III. Noncrystalline statoliths were found from brackish water (*Rhopalophthalmus*) to the deep sea (*Boreomysis*), with the greatest numbers in depths of 201–2000 m. The frequency of fluorite mineralization increased from freshwater to marine environments, with a maximum in the photic zone (0–200 m). On the contrary, vaterite was most common in fresh water and completely absent in the deep sea (Table IIIa). With respect to frequency of mineral types in different biota (Table IIIb), vaterite prevailed in freshwater organisms but fluorite was the dominant form in all remaining aquatic biota.

The microanalytical determinations gave only qualitative results. More elements were recorded in noncrystalline and fluorite statoliths than in vaterite statoliths. Species studied were *Boreomysis megalops* (Na, Mg, S, Ca), *B. microps* (Mg, Si, S, Cr, Fe, Ni), and *Rhopalophthalmus terranatalis* (Mg, S, Ca, Fe, Cu) with noncrystalline statoliths; *Katerythrops oceanae* (F, Mg, Si, P, S, Ca, Zn), *Pseudomma latiphthalmum* (F, Mg, P, S, Ca, Cr, Zn), *Idiomysis tsurnamali* (F, P, Ca), and *Paramysis arenosa* (F, K, Ca) with fluorite; *P. lacustris tanaitica* (P, S, Ca, Cu), *Schistomysis assimilis* (P, S, Ca), and *Limnomysis benedeni* (P, S, Ca) with vaterite. In *S. assimilis* the presence of Ni and Cu varied between populations (present in Gulf of Venice; absent in Gulf of Salerno) and among individuals (n = 6). In *L. benedeni* the presence of Cu varied among individuals (n = 4).

Discussion

Our study covers about 17% of the extant species described worldwide for the family Mysidae; this includes

Table III

Occurrence (% populations) of mineral types of mysid statoliths in different aquatic biota

A. Percentages of biota with respect to mineral types

Type	n	Freshwater %	Brackish %	Marine 0–200 m %	Marine 201–2000 m %
Noncrystalline	8	0	13	13	75
Fluorite	150	3	7	65	24
Vaterite	21	43	33	24	0

B. Percentages of mineral types with respect to biota

Type	Freshwater n = 14	Brackish n = 19	Marine 0–200 m n = 104	Marine 201–2000 m n = 42
Noncrystalline %	0	5	1	14
Fluorite %	36	58	94	86
Vaterite %	64	37	5	0

34% of the genera and all subfamilies. All oceans and shelf areas of all continents are represented. Special emphasis is placed on zoogeographically important areas such as the Black Sea, the Mediterranean, the Red Sea, the Caribbean, Japan, Tasmania, and the Antarctic. Species are littoral, coastal, or oceanic (epi-, meso-, and bathypelagic); estuarine, limnic, or cave dwelling. Results are thus highly representative of the mysid fauna of the world, with the reservation that European species are overrepresented.

Three main types of statoliths were identified: those without crystalline components (organic statoliths), and those mineralized with either fluorite or calcium carbonate (vaterite or calcite).

As in other x-ray diffraction studies, qualitative microanalysis was used to provide supplementary information. The determinations showed a high diversity of trace elements. When a mysid molts, its statocyst cavity is open to ambient water; therefore, we cannot exclude the possibility that the presence of some elements in marine and brackish-water species is a residual of sea salt that has been enclosed during statolith formation. The presence of sulfur in most statoliths coincides with the finding of sulfated mucopolysaccharides in fluorite statoliths (Espeel, 1987). In *Boreomysis microps*, the absence of calcium in the noncrystalline statoliths further indicates their nonmineralic composition. The absence of fluorine in all examined vaterite statoliths suggests that vaterite and fluorite statoliths have different mineralization patterns.

Noncrystalline statoliths are characteristic of the Boreomysinae and the Rhopalophthalminae, two subfamilies considered primitive among Mysidae (Tattersall and Tattersall, 1951; Schlacher *et al.*, 1992).

Fluorite precipitation represents the most frequent mineral-forming process occurring in statocysts of Mysidae. It remains unclear why these animals are bearing the expense of concentrating fluorine, an element present in small quantities (1.3 mg/l in seawater (35‰) and almost absent in fresh water). This is especially remarkable if one considers the large size of fluorite statoliths, which have diameters about 1–4% of body length.

Mineralization with $CaCO_3$ is known in both Recent and fossil statoliths. The noteworthy aspect of this very common form of biomineralization is that extant forms produce vaterite. Precipitation of this hexagonal metastable polymorph of crystalline $CaCO_3$ may have biological significance by favoring rapid statolith formation after each molt (Ariani *et al.*, 1981). In fact, vaterite is often precipitated during the regeneration of the aragonitic shells of mollusks, when sudden mobilization of calcium is necessary (Watabe *et al.*, 1976). Considering the metastable nature of vaterite and the absence of calcite in Recent species, it seems likely that calcite in fossil specimens was formed by phase transformation of vaterite during or after the process of fossilization. Voicu (1981) assigned Miocene calcite statoliths to *Paramysis*, a genus that precipitates vaterite in Recent forms of the Black Sea area (Table I). His assumption that the Recent species *Paramysis kroeyeri* and *P. kessleri sarsi* produce calcite was not confirmed by our finding of vaterite in both species.

Conspecific populations from different geographical areas and different biota show identical crystallographic characteristics (Table I); thus mineral composition of statoliths appears to be a definite specific character. The presence of an organic matrix in all types of statoliths (Wittmann *et al.*, 1993) suggests that the mineral type is matrix mediated and under genetic control, as in fish otoliths (Gauldie, 1986). Genes controlling the mineral type of vertebrate otoconia have important functions in the physiology of the inner ear (Mulligan and Gauldie, 1989). These observations render discussions on the adaptive meaning of mineral type rather difficult, because natural selection may act via complex epigenetic patterns.

In contrast to the similarity of mineral type on the intraspecific level, either vaterite or fluorite may be found when congeneric species or closely related genera of the tribe Mysini are compared. Table III confirms the dominant role of vaterite in fresh water and of fluorite in seawater. The finding (Enbysk and Linger, 1966) of fluorite statoliths in subfossil shelf sediments of northwestern America fits this picture. Vaterite statoliths are rare in marine water. All marine forms with vaterite statoliths also inhabit brackish or fresh waters (Table I). According to Voicu (1981), in seawater the function of the static organ demands the precipitation of a mineral with a greater specific gravity (fluorite, 3.2) than in fresh water (calcite, 2.7; we add vaterite, 2.5). Ariani *et al.* (1983) note that the precipitation of fluorine in fresh water may be difficult or impossible when fluorine concentrations are low. Nevertheless, four freshwater species, *Mysis relicta*, *Taphromysis lousianae*, *Diamysis pengoi*, and *Troglomysis vjetrenicensis*, precipitate fluorite. This is especially remarkable for *D. pengoi* and *T. vjetrenicensis*, because they are closely related to *D. bahirensis*, an extremely euryhaline form that occurs mainly in brackish waters and produces vaterite. The ecological meaning of this situation is still obscure.

Biogeographical correlations may be established based on the fact that vaterite statoliths are found only in two groups of closely related genera of Mysini, the '*Diamysis* group' (*Diamysis*, *Limnomysis*, and *Antromysis*) and the '*Paramysis* group' (*Paramysis*, *Katamysis*, and *Schistomysis*). Both groups are characterized by features of antennal scale and male pleopods. Vaterite is found in *Hemimysis*, which shows intermediate morphological features. Most Recent vaterite-forming species inhabit the Ponto-Caspian region (Table I), where calcareous mysid statoliths largely occur (Voicu, 1974; Fuchs, 1979) in Miocene deposits of the brackish Paratethys. The Caribbean genus *Antromysis* does not fit this pattern, but it is a vicariant of the European genus *Diamysis*.

The biogeography of calcareous statoliths and their predominant role in fresh water are mutually dependent. About one-third of the world fauna of freshwater Mysidae is endemic to the Ponto-Caspian region, where the Danube river alone is inhabited by 10 species. Vaterite is found in 78% species (n = 9; see Table 1) of the tribe Mysini in the Black Sea including adjacent waters. Based on faunal composition, a similar value is expected for the Caspian Sea. Corresponding values are 30% (n = 10) for the Mediterranean, 17% (n = 24) for the Atlantic, and 0% (n = 22) for all remaining seas and oceans of the globe. From species composition in the Baltic, we expect that vaterite is found only in species introduced by man (Köhn, 1992) from the Ponto-Caspian (*Hemimysis anomala, Limnomysis benedeni,* and *Paramysis lacustris*).

The earliest fossil records of Mysidacea are Lophogastrida (or nearly so) from Carboniferous to Jurassic sediments (see compilation in Tattersall and Tattersall, 1951). Most Recent forms belonging to this suborder have an oceanic life habit. Together with several small families (Petalophthalmidae, Stygiomysidae, and Lepidomysidae) within the suborder Mysida, they have conserved the ancestral mysidacean morphotype, characterized by seven pairs of brood plates, (nearly) unmodified male pleopods, and the absence of statocysts.

No early fossil records are available for the species-rich family Mysidae, which has statocysts in the endopods of uropods as its most important autapomorphic feature. As discussed by Schlacher *et al.* (1992), the subfamilies Boreomysinae (pelagic) and Rhopalophthalminae (benthopelagic) have conserved certain plesiomorphic features such as subdivided exopods of uropods and biramous and many-segmented male pleopods or, as in Boreomysinae, seven pairs of brood plates. In both subfamilies, the statoliths are exclusively noncrystalline (Table 1). The apparent correlation with plesiomorphic characters suggests that organic statoliths may have preceded mineralic ones. The probable ancestral status of nonmineralized statoliths is also supported by the observations of Ariani *et al.* (1982) on the ontogenetic development of calcareous statoliths.

The late appearance of mineralic statoliths in fossil history (Lower Miocene according to Voicu, 1981) points to a post-Cretaceous origin of modern Mysidae (Siriellinae, Gastrosaccinae, Mysinae, and Mysidellinae), which are characterized by two to three pairs of brood plates, reduced pleopods in females, and specialized pleopods in males. Most Recent species have fluorite statoliths (Table 1); these constitute the bulk of the benthopelagic to benthic forms inhabiting coastal and littoral zones of all oceans.

Our evolutionary scheme is aligned with the theoretical considerations of Buddenbrock (1914) on the biological meaning of static organs in crustaceans. Besides control of body position, the main adaptive value of such organs is support of visual orientation in the complex spatial structure found in benthopelagic to benthic habitats; this function is less important in oceanic habitats where orientation towards light source is paramount. In fact, Neil (1975) gave experimental evidence that the statocysts of mysids stabilize the visual perceptive field through statocyst modulation of the optokinetic eyestalk movements. Biometrical observations by Wittmann *et al.* (1990) fit this concept by showing that, on the average, blind mysids or those with reduced eyes have smaller statoliths than those with well-developed eyes.

Both the scarcity of mysid statoliths outside Paratethyan sediments and the biogeography of Recent species suggest that $CaCO_3$ statoliths developed in fresh to brackish waters of the Ponto-Caspian region during the Miocene. A large marine to brackish basin, the Paratethys, covered the region during that period. In the late Miocene, salinities gradually decreased in peripheral areas such as the Vienna Basin (Fuchs, 1979). During the Pleistocene, conditions in the Black Sea area varied between completely freshwater during glaciations and brackish during interglacial periods (Hsü, 1978). These events may have favored the evolution of a rich brackish to freshwater fauna.

The few vaterite-forming species outside the Ponto-Caspian (Table 1) have close relatives there and thus are probably of the same origin. Such relationships are obvious for certain members of the *Diamysis* group (Wittmann, 1992). The problem arises, however, that most vaterite-forming species have close relatives that form fluorite. The occurrence of both mineral types in congeneric species of *Hemimysis, Diamysis, Paramysis,* and *Schistomysis* suggests that vaterite evolved from fluorite in at least four parallel lines. The only reasonable explanation appears to be homoiology—that is, analogy on the basis of homology: the common ancestors may have evolved physiological or morphological predispositions favoring a phylogenetically rapid shift of statolith mineral composition from fluorite to calcium carbonate.

Statolith crystallography in the Mysidae seems to reflect two elements: first, the morphological differentiation between two primitive subfamilies, the Boreomysinae and the Rhopalophthalminae, with organic statoliths and all remaining taxa with mineralized statoliths; and second, ecophysiological differences between marine forms with fluorite and freshwater forms with vaterite. These elements offer parallels to those advanced by Carlström (1963) for the vertebrates, where the mineral composition of otoliths reflects first, the anatomical division in two main groups, the Agnatha with phosphate and the Gnathostomata with carbonate; and second, the differentiation between coldblooded forms with aragonite or vaterite and warm-blooded ones with calcite. The more recent discovery of calcite in certain amphibians (Marmo *et al.*, 1983) suggests that the appearance of calcite may rather mark the transition from an aquatic to a terrestrial mode of live.

Acknowledgments

We are greatly indebted to members of the "Mysid Research Group" for exchange or donation of mysid material: T. E. Bowman (Washington), T. Brattegard (Blomsterdalen), G. Fenton (Hobart), J. Mauchline (Oban), S. M. Lussier (Narragansett), M. Murano (Tokyo), J. C. Sorbe (Arcachon), and T. Wooldridge (Port Elizabeth). We also thank G. Voicu (Bucarest) for the generous donation of fossil statoliths. The Division of Ultrastructure, Zool. Inst. Vienna, and Lab. Micr. Elettronica, Dip. Sci. Terra (Naples), kindly provided scanning electron microscopy and microanalytical facilities. Part of the material was collected during the Antarctic expedition ANT VIII/5 of the RV *Polarstern*.

Literature Cited

Ariani, A. P., F. Marmo, G. Balsamo, and E. Franco. 1981. Vaterite in the statoliths of a mysid crustacean (*Diamysis bahirensis*). *Annuar. Ist. Mus. Zool. Univ. Napoli* **24:** 69–78.

Ariani, A. P., F. Marmo, G. Balsamo, G. Cesaro, and N. Maresca. 1982. Prime osservazioni sullo sviluppo degli statoliti di Crostacei Misidacei. *Annuar. Ist. Mus. Zool. Univ. Napoli* **25:** 327–341.

Ariani, A. P., F. Marmo, G. Balsamo, E. Franco, and K. J. Wittmann. 1983. The mineral composition of statoliths in relation to taxonomy and ecology in mysids. *Rapp. Comm. Int. Mer Médit.* **28**(6): 333–336.

Bethe, A. 1895. Die Otocyste von *Mysis*. *Zool. Jb. Anat. Ontog.* **8:** 544–564.

Buddenbrock, W. von. 1914. Über die Orientierung der Krebse im Raum. *Zool. Jb. Allg. Zool.* **34:** 479–514.

Carlström, D. 1963. A crystallographic study of vertebrate otoliths. *Biol. Bull.* **125:** 441–463.

Eobysk, B. J., and F. L. Linger. 1966. Mysid statoliths in shelf sediments off Northwest America. *J. Sediment. Petrol.* **36:** 839–840.

Espeel, M. F. 1987. On the fine structure of the statolith and the caudal statocyst gland of the mysid shrimp *Neomysis integer* (Leach, 1814) (Crustacea, Mysidacea). *Meded. K. Acad. Wet., Lett. Sch. Kunst. België* **49**(1): 95–109.

Fuchs, R. 1979. Das Vorkommen von Statolithen fossiler Mysiden (Crustacea) im obersten Sarmatien (O-Miozän) der Zentralen Paratethys. *Beitr. Paläont. Österreich* **6:** 61–69.

Gauldie, R. W. 1986. Vaterite otoliths from chinook salmon (*Oncorhynchus tshawytscha*). *New Zealand J. Mar. Freshw. Res.* **20:** 209–217.

Gauldie, R. W. 1990. Vaterite otoliths from the opah: *Lampris immaculatus* and two species of sunfish, *Mola mola* and *M. ramsayi*. *Acta Zool.* **71**(4): 193–199.

Hsu, K. J. 1978. When the Black Sea was drained. *Sci. Am.* **238**(5): 53–63.

Jander, R. 1962. The swimming plane of the crustacean *Mysidium gracile* (Dana). *Biol. Bull.* **122:** 380–390.

Köhn, J. 1992. Mysidacea of the Baltic Sea—state of the art. Pp. 5–23 in *Taxonomy, Biology and Ecology of (Baltic) Mysids (Mysidacea, Crustacea)*, J. Köhn, M. B. Jones, and A. Moffat, eds. Univ. Rostock.

Lowenstam, H. A. 1981. Minerals formed by organisms. *Science* **211:** 1126–1131.

Lowenstam, H. A., and D. McConnell. 1968. Biologic precipitation of fluorite. *Science* **162:** 1496–1498.

Maissuradze, L. S., and G. Popescu. 1987. Carpatho-Caucasian comparative study of Sarmatian Mysids. *D. S. Inst. Geol. Geofiz.* **72–73**(3): 75–80.

Marmo, F., G. Balsamo, and E. Franco. 1983. Calcite in the statoconia of amphibians. A detailed analysis for the frog *Rana esculenta*. *Cell Tissue Res.* **233:** 35–43.

Mulligan, K. P., and R. W. Gauldie. 1989. The biological significance of the variation in crystalline morph and habit of otoconia in elasmobranchs. *Copeia* **1989**(4): 856–871.

Neil, D. M. 1975. Statocyst control of eyestalk movements in mysid shrimps. *Fortschr. Zool.* **23:**98–109.

Schlacher, T. A., K. J. Wittmann, and A. P. Ariani. 1992. Comparative morphology and actuopalaeontology of mysid statoliths (Crustacea, Mysidacea). *Zoomorphology* **112:** 67–79.

Tattersall, W. M., and O. S. Tattersall. 1951. *The British Mysidacea.* Ray Society, Publ. 136, London, 460 pp.

Voicu, G. 1974. Identification des Mysidés fossiles dans les dépôts du Miocène supérieur de la Paratéthys Centrale et Orientale et leur importance paléontologique, stratigraphique et paléogéographique. *Geol. Carpath.* **25:** 231–239.

Voicu, G. 1981. Upper Miocene and Recent mysid statoliths in Central and Eastern Paratethys. *Micropaleontology* **27:** 227–247.

Watabe N., V. R. Meenakshi, P. L. Blackwelder, E. M. Kurtz, and D. G. Dunkelberger. 1976. Calcareous spherules in the gastropod *Pomacea paludosa*. Pp. 283–308 in *The Mechanisms of Mineralization in the Invertebrates and Plants*, N. Watabe and K. M. Wilbur, eds. Univ. South Carolina Press, Columbia.

Wittmann, K. J. 1992. Morphogeographic variations in the genus *Mesopodopsis* Czerniavsky with descriptions of three new species (Crustacea, Mysidacea). *Hydrobiologia* **241:** 71–89.

Wittmann, K. J., A. P. Ariani, and A. Stanzione. 1990. Implicazioni tassonomiche ed ecologiche di alcune caratteristiche biometriche degli statoliti dei Misidacei. *Oebalia* **16–2**(Suppl.): 805–807.

Wittmann, K. J., T. A. Schlacher, and A. P. Ariani. 1993. Structure of Recent and fossil mysid statoliths (Crustacea, Mysidacea). *J. Morphol.* **215:** 31–49.